



SPACOMM 2024

The Sixteenth International Conference on Advances in Satellite and Space
Communications

ISBN: 978-1-68558-179-4

May 26 - 30, 2024

Barcelona, Spain

SPACOMM 2024 Editors

Oliver Michler, Technical University Dresden, Germany

Nadia Kortas, National Aeronautics and Space Administration (NASA), USA

SPACOMM 2024

Forward

The Sixteenth International Conference on Advances in Satellite and Space Communications (SPACOMM 2024), held between May 26-30, 2024 in Barcelona, Spain, continued a series of events attempting to evaluate the state of the art on academia and industry on the satellite, radar, and antennas based communications bringing together scientists and practitioners with challenging issues, achievements, and lessons learnt.

Significant efforts have been allotted to design and deploy global navigation satellite communications systems, Satellite navigation technologies, applications, and services experience still challenges related to signal processing, security, performance, and accuracy. Theories and practices on system-in-package RF design techniques, filters, passive circuits, microwaves, frequency handling, radars, antennas, and radio communications and radio waves propagation have been implemented. Services based on their use are now available, especially those for global positioning and navigation. For example, it is critical to identify the location of targets or the direction of arrival of any signal for civilians or on-purpose applications; smart antennas and advanced active filters are playing a crucial role. Also progress has been made for transmission strategies; multiantenna systems can be used to increase the transmission speed without need for more bandwidth or power. Special techniques and strategies have been developed and implemented in electronic warfare target location systems.

We welcomed academic, research and industry contributions. The conference had the following tracks:

- Satellite and space communications
- Satellites and nano-satellites
- Satellite/space communications-based applications

We take here the opportunity to warmly thank all the members of the SPACOMM 2024 technical program committee, as well as all the reviewers. The creation of such a high quality conference program would not have been possible without their involvement. We also kindly thank all the authors who dedicated much of their time and effort to contribute to SPACOMM 2024. We truly believe that, thanks to all these efforts, the final conference program consisted of top quality contributions.

We also thank the members of the SPACOMM 2024 organizing committee for their help in handling the logistics and for their work that made this professional meeting a success.

We hope that SPACOMM 2024 was a successful international forum for the exchange of ideas and results between academia and industry and to promote further progress in the domain of satellites and space communications. We also hope that Barcelona provided a pleasant environment during the conference and everyone saved some time to enjoy the historic charm of the city.

SPACOMM 2024 Chairs

SPACOMM Steering Committee

Timothy T. Pham, Jet Propulsion Laboratory - California Institute of Technology, USA

Stelios Papaharalabos, u-blox Athens, Greece

Oliver Michler, Technical University Dresden, Germany

SPACOMM Publicity Chairs

Laura Garcia, Universidad Politécnica de Cartagena, Spain

Sandra Viciano Tudela, Universitat Politecnica de Valencia, Spain

SPACOMM 2024

Committee

SPACOMM Steering Committee

Timothy T. Pham, Jet Propulsion Laboratory - California Institute of Technology, USA
Stelios Papaharalabos, u-blox Athens, Greece
Oliver Michler, Technical University Dresden, Germany

SPACOMM 2024 Publicity Chairs

Laura Garcia, Universidad Politécnica de Cartagena, Spain
Sandra Viciano Tudela, Universitat Politecnica de Valencia, Spain

SPACOMM 2024 Technical Program Committee

Zahir A. Hussein Alsulaimawi, Oregon State University, USA
Suayb S. Arslan, MEF University, Turkey
Michael Atighetchi, Raytheon BBN Technologies, USA
Adrian S. Barb, Penn State University, USA
Peter Baumann, Jacobs University, Germany
Raed S.M Daraghmah, Palestine Technical University, Palestine
Arun Das, Arizona State University, USA
Yiping Duan, Tsinghua University, China
Nour El Madhoun, Laboratoire Sécurité & Système de l'EPITA (LSE), France
Mohamed A. Elshafey, Military Technical College, Cairo, Egypt
Luiz Carlos Gadelha de Souza, Federal University of ABC, Brazil
Gregory Hellbourg, International Center for Radio Astronomy Research | Curtin University, Western Australia
Sundararaja Sitharama Iyengar, Florida International University, USA
Seifallah Jardak, Bristol Research & Innovation Laboratory - Toshiba, UK
Vladimir Karaev, Institute of Applied Physics of Russian Academy of Sciences, Russia
Baris Kazar, Oracle America Inc., USA
Mohamed Khalaf-Allah, Friedrich-Alexander University of Erlangen-Nuremberg, Germany
Adil Hakeem Khan, Nation College of Engineering and Technology, Guna, India
Arash Komae, Southern Illinois University, Carbondale, USA
Nadia Kortas, NASA - Space Communication and Navigation Program (SCaN), USA
Pablo Madoery, Universidad Nacional de Córdoba, Argentina
Krešimir Malarić, University of Zagreb, Croatia
Michael P. McGuire, Towson University, USA
Oliver Michler, Technical University Dresden, Germany
Sara Migliorini, Università degli Studi di Verona, Italy
Nelli Mosavi, Johns Hopkins University, USA
Nitin Muchhal, Institute of Information Technology (J.I.I.T) Noida, India
Tathagata Mukherjee, The University of Alabama in Huntsville, USA

David N. Amanor, Intel Corporation, USA
Brian Niehoefer, TÜV Informationstechnik GmbH, Germany
Nele Noels, Ghent University, Belgium
W. David Pan, University of Alabama in Huntsville, USA
Krishna Pande, National Chiao Tung University, Taiwan
Cathryn Peoples, Ulster University, UK
Timothy Pham, Jet Propulsion Laboratory, USA
Ermanno Pietrosemoli, The Abdus Salam International Centre for Theoretical Physics (ICTP), Italy
Alexandru Rusu, University Politehnica of Bucharest, Romania
Takeyasu Sakai, Electronic Navigation Research Institute - National Institute of Maritime, Port and Aviation Technology, Japan
Anoop Kumar Shukla, Manipal Academy of Higher Education, India
Gulab Singh, Indian Institute of Technology Bombay, India
Predrag Spasojevic, Rutgers University, USA
Cristian Lucian Stanciu, University Politehnica of Bucharest, Romania
Salvatore Stramondo, Istituto Nazionale di Geofisica e Vulcanologia, Italy
Robert Sundberg, Spectral Sciences Inc., USA
Lahouaria Tabti, Center of Space Techniques/Algerian Space Agency, Algeria
Veeru Talreja, West Virginia University, USA
Yuriy Titchenko, Institute of Applied Physics of the Russian Academy of Sciences, Russia
Stefanos Vrochidis, Information Technologies Institute, Greece
Tin Vu, Microsoft, USA
Xiao Wang, Boston University, USA
Hong Wei, University of Maryland, USA
Yuhang Zang, Nanyang Technological University, Singapore
Yimin Daniel Zhang, Temple University, USA
Yunfan Gerry Zhang, Independent Researcher, USA
Zenghui Zhang, Shanghai Jiao Tong University, China
Guoqing Zhou, Guilin University of Technology, China

Copyright Information

For your reference, this is the text governing the copyright release for material published by IARIA.

The copyright release is a transfer of publication rights, which allows IARIA and its partners to drive the dissemination of the published material. This allows IARIA to give articles increased visibility via distribution, inclusion in libraries, and arrangements for submission to indexes.

I, the undersigned, declare that the article is original, and that I represent the authors of this article in the copyright release matters. If this work has been done as work-for-hire, I have obtained all necessary clearances to execute a copyright release. I hereby irrevocably transfer exclusive copyright for this material to IARIA. I give IARIA permission to reproduce the work in any media format such as, but not limited to, print, digital, or electronic. I give IARIA permission to distribute the materials without restriction to any institutions or individuals. I give IARIA permission to submit the work for inclusion in article repositories as IARIA sees fit.

I, the undersigned, declare that to the best of my knowledge, the article does not contain libelous or otherwise unlawful contents or invading the right of privacy or infringing on a proprietary right.

Following the copyright release, any circulated version of the article must bear the copyright notice and any header and footer information that IARIA applies to the published article.

IARIA grants royalty-free permission to the authors to disseminate the work, under the above provisions, for any academic, commercial, or industrial use. IARIA grants royalty-free permission to any individuals or institutions to make the article available electronically, online, or in print.

IARIA acknowledges that rights to any algorithm, process, procedure, apparatus, or articles of manufacture remain with the authors and their employers.

I, the undersigned, understand that IARIA will not be liable, in contract, tort (including, without limitation, negligence), pre-contract or other representations (other than fraudulent misrepresentations) or otherwise in connection with the publication of my work.

Exception to the above is made for work-for-hire performed while employed by the government. In that case, copyright to the material remains with the said government. The rightful owners (authors and government entity) grant unlimited and unrestricted permission to IARIA, IARIA's contractors, and IARIA's partners to further distribute the work.

Table of Contents

Integrating Satellite Constellation and Mobile Operations for Non-Terrestrial Networks: Preliminary Results of Dynamic Scheduling <i>Arnau Singla, Franco Criscola, David Canales, Anna Calveras, Juan A. Fraire, and Joan A. Ruiz-de-Azua</i>	1
Enhanced Path Reliability of Contact Graph Routing through a Cognitive Extension <i>Ricardo Lent</i>	7
Spectral Target Detection at Twilight <i>Robert Sundberg</i>	13
Improved Method for Telemetry Data Processing in LEO Satellite <i>Dongseok Chae</i>	17

Integrating Satellite Constellation and Mobile Operations for Non-Terrestrial Networks: Preliminary Results of Dynamic Scheduling

Arnau Singla

*Space Communications Research Group
i2CAT Foundation
Barcelona, Spain
email: arnau.singla@i2cat.net*

Franco Criscola

*Aerospace Engineering
Embry-Riddle Aeronautical University
Daytona Beach, United States
email: CRISCOLF@my.erau.edu*

David Canales

*Aerospace Engineering
Embry-Riddle Aeronautical University
Daytona Beach, United States
email: CANALED4@erau.edu*

Anna Calveras

*Network Engineering
Universitat Politècnica de Catalunya
Barcelona, Spain
email: anna.calveras@upc.edu*

Juan A. Fraire

*Inria/INSA Lyon, CITI
CONICET-UNC
Villeurbanne, France
email: juan.fraire@inria.fr*

Joan A. Ruiz-de-Azua

*Space Communications Research Group
i2CAT Foundation
Barcelona, Spain
email: joan.ruizdeazua@i2cat.net*

Abstract—The integration of terrestrial networks with Non-Terrestrial Networks requires a comprehensive management framework to address the mutual impact between satellite operations and network services. Past research by the authors introduced the Constellation Management System (CMS) as a solution, facilitating optimized plans for both satellite and network operators. This paper extends prior work by focusing on enhancing the adaptability of the CMS through dynamic execution methodologies, particularly by integrating telemetry feedback. The study presents a dynamic execution framework and a sequence diagram outlining the rescheduling process. Validation through telemetry emulation demonstrates the system's agility in responding to telemetry variations and the value of this new architecture using the CMS dynamically. Initial findings indicate a throughput enhancement of 10% with the implementation of a closed-loop approach compared to an open-loop approach. This research advances satellite constellation operations management towards automated communications, enhancing adaptability and robustness in unpredictable and constantly changing environments.

Keywords—NTN; operations scheduling; satellite IoT; closed-loop optimization; 3GPP.

I. INTRODUCTION

Over the last decade, the landscape of the space economy has undergone significant changes. While previously limited to governmental agencies mainly founded by public investment, technological advancements have increased private investment in space missions. This impact has been notable in Earth Observation (EO) and satellite telecommunications missions [1] [2]. One of the telecommunications domains poised to leverage the vast potential of satellite constellations is the realm of Internet of Things (IoT) [3]. Established terrestrial IoT networks stand to benefit significantly from augmented satellite coverage, particularly in remote and inaccessible regions, thereby extending ubiquitous global connectivity ser-

vices [4]. This expansion proves especially valuable in areas where conventional IoT infrastructure faces technical and/or economic constraints, fostering a myriad of new application prospects [5].

The advent of 6th Generation (6G) technology heralds an era of expansive deployment of massive IoT networks, necessitating global coverage [6]. Consequently, there has been an effort to integrate satellite systems with ground-based telecommunications infrastructures, a trend underscored by initiatives, such as the Third Generation Partnership Project (3GPP) [7]. Notably, standardization efforts have led to the inclusion of spacecraft and aircraft within a 5th Generation (5G)-compliant architecture, thereby establishing them as Non-Terrestrial Networks (NTN) [8]. This represents an initial step toward integrating satellite systems with terrestrial infrastructure. Building upon this foundation, there is a growing emphasis on extending radio protocols, such as New Radio (NR) [9] and Narrow-Band Internet of Things (NB-IoT) [10], to accommodate satellite connectivity within the existing terrestrial framework, facilitating seamless integration of satellite systems into the broader telecommunications ecosystem [11].

The proposed solutions for satellite NB-IoT in the literature are mainly focused on Low Earth Orbit (LEO) constellations [12]. These constellations, often deployed for global coverage, may employ Store and Forward (S&F) mechanisms for data delivery in sparse constellations [13], adapting its protocols to 3GPP NB-IoT [14]. However, managing the operations of these LEO constellations, especially for telecom purposes, poses substantial challenges. The complexity arises from integrating satellite operations with mobile network operations. Examples are the diverse elements in a heterogeneous environment, the resource-constrained nature of satellite platforms, and the necessity to incorporate mobile network business

criteria into satellite operations, among others.

Recognizing the need for efficient and autonomous management systems for telecom LEO constellations is crucial in this context [15]. Although available, traditional satellite-by-satellite operations and commercial solutions often fall short of meeting the intricate requirements of this evolving landscape. As current operations management research predominantly focuses on EO missions, there is a call for tailored solutions to address the unique challenges of the telecom use case effectively. Towards this goal, we have designed and developed an autonomous and reactive constellation management system, integrated with the Core Network (CN), to enhance the NTN architecture by extending IoT services with a LEO satellite constellation using S&F. The innovative system and its architecture are elaborated upon in this paper by the same individuals as the present study [16]. This study focuses on extending the previous capabilities of the Constellation Management System (CMS) and its dynamic capabilities, showcasing the autonomous integration of satellite telemetry feedback (e.g., power, memory) during continuous operation.

The rest of the paper is structured as follows. Section II explains the motivation behind a reactive scheduling system. Section III briefly presents the CMS. Then, Section IV describes the novel proposed dynamic execution of the CMS. After that, Section V depicts the scenario used for dynamic validation. The most relevant results to validate the execution are presented in Section VI. Finally, Section VII concludes the work and highlights possible future research topics.

II. PROBLEM STATEMENT

Addressing the intricacies of a S&F LEO constellation as IoT-NTN, the CMS confronts numerous challenges from an operations perspective [17]. These scenarios often present highly heterogeneous environments where various entities with diverse priorities intersect. The optimization criteria of satellite and network/service operators differ, yet they are interlinked. Nevertheless, the CMS aims to devise a contact plan for satellites that optimally balances the requirements of both resource efficiency and the business criteria set forth by the service provider. It is essential to note that when extending existing terrestrial networks, operations must also be integrated into systems with specific standards (e.g., 3GPP).

Given the complexity of constellations characterized by discontinuous connectivity and limited onboard resources [2], centralized operations planning and optimization become imperative. However, the telecom scenario's unpredictability poses a challenge in planning, prompting the need for strategies to compensate for this evolving behavior. Viable solutions include utilizing a highly accurate traffic model [18] [19]. Nevertheless, a satellite constellation can serve different types of users or offer different services, making the traffic model not a suitable solution. So, as not to depend solely on the traffic model, another approach is enhancing the scheduling system's reactivity by dynamically incorporating feedback from the scenario and continually re-configuring the constellation contact plan, following a closed-loop optimization approach [20].

This work primarily focuses on addressing the latter challenge by assessing the impact of integrating telemetry feedback on the planned tasks' completion status and the constellation satellites' present resource levels. This evaluation is conducted using preliminary results obtained from a case study.

The telemetry feedback methodology has previously undergone testing in the GOMX-4 mission, aimed at refining battery prediction for the mission's dual satellites. Authors in [21] and [22] describe the GOMSPACE Hands-Off Operations Platform (HOOP), a commercial automatic satellite operations tool provided by the company. While sharing a fundamental concept with the CMS, HOOP is specifically optimized for EO missions, particularly in its scheduling engine. Notably, the referenced studies primarily focused on battery readings within their telemetry feedback, omitting considerations of scenario variability and disturbances. This current research contributes to the telemetry feedback approach, extending its application to telecommunications scenarios and incorporating additional layers to account for failed tasks and other resources, such as memory. This enhances the traffic model's precision and the management system's robustness to disturbances. The novelty of this work is optimizing satellite operations for telecom IoT services using a task scheduling approach and enhancing it with reactive planning to overcome the scenario unpredictability challenge.

III. CONSTELLATION MANAGEMENT SYSTEM

The CMS is an independent satellite operations management system capable of integrating and orchestrating various agents by generating a resource- and business-aware schedule. This schedule, in turn, forms the foundation for generating: (1) a contact plan used by the satellite forwarding system, (2) an operations plan for the Mission Provider (MP), (3) a CN plan to coordinate traffic to and from terrestrial networks, and (4) a Ground Station Network (GSN) plan to synchronize the ground segment. The modular architecture of the CMS is represented in Figure 1.

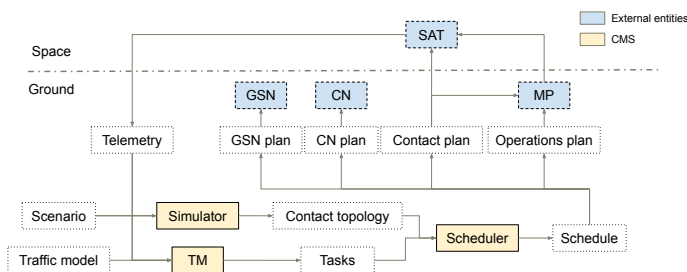


Figure 1. CMS global architecture.

The operator introduces scenario elements to the simulator module and the traffic model to the Task Manager (TM) module. The simulator, in turn, is entrusted with generating the contact topology of the problem, propagating contact windows between satellites and other elements (e.g., Ground Station (GS) or Service Area (SA)). Simultaneously, the TM produces input tasks for the scheduler module. The scheduler

module employs a constraint satisfaction engine and artificial intelligence search algorithms to optimize task assignments.

The entire process and post-processing of the schedule into various plans and distributing them to their respective agents is overseen by the Plan Executor (PE) module. This module is responsible for dynamically controlling the execution of the CMS and managing the inputs and outputs of the system. Earlier work focused on the scheduler module, its model, and mathematical formulation [16]. This research focuses on the rest of the support modules surrounding the scheduler and their interactions to achieve reactive planning.

IV. DYNAMIC SCHEDULING

This section describes the dynamic execution process of the CMS, along with the call flow process initiated upon triggering a reschedule. Figure 2 visually represents this dynamic execution through a sequence diagram.

Step 1 is a reschedule trigger to the plan executor. This trigger might come from different situations, such as (1) new inputs to the database, (2) a change in the scenario elements (e.g., a new SA), (3) a periodic time according to the scheduled time horizon, or (4) a manual trigger from the operator. The PE then starts the dynamic scheduling sequence by requesting the contact windows between the scenario satellites and the rest of the elements (GS, SA, and other satellites). The current scenario elements are stored in the simulator database. As such, if any of the scenario elements has changed, the PE will first store the new elements in the database (step 2) and then proceed to request a contact window search to the simulator module (step 3). Upon receiving a Windows request, the simulator shall fetch the scenario elements from its database, compute the contact windows, and store them in the database (steps 4-7). Finally, the simulator responds to the PE with the list of contact windows (step 8). If the scenario remains the same, then the PE directly requests the list of contact windows to the simulator database (steps 9-10). The database is periodically fed by the simulator with future contact windows. This way, the PE does not need to wait for the scenario propagation when requesting the contact windows, should the scenario remain the same.

Once the PE has the contact windows, the initial tasks are requested to the TM module (step 11). The TM requires the contact windows to generate the expected tasks according to the traffic model used. Before new tasks are computed, the TM keeps the assigned tasks of the previous schedule, which are yet to happen. The TM fetches the previous schedule and its timestamp from the schedule database (steps 12-13). Furthermore, the TM adds to the initial task list all previously assigned tasks reported to fail. The TM fetches the failed tasks from the telemetry database (steps 14-15). After computing the new tasks according to the traffic model and the scenario windows (step 16), the TM responds to the PE with the task list (step 17). In our task management system, each task is associated with an expiration date parameter, indicating when the data within the task becomes outdated. This parameter remains constant even if the task is rescheduled. As a result,

our scheduler prioritizes tasks that are nearing their expiration date over newer tasks with later expiration dates. This ensures that we address impending data expiration and maintain data relevance within our system.

After that, the only thing required before sending the optimization request to the scheduler is to set the initial resources of each satellite. Towards that purpose, the PE fetches the predicted resources from the previous schedule stored in the schedule database (steps 18-19). The PE also fetches the latest telemetry updates regarding resources for each satellite from the telemetry database (steps 20-21). With all that information, the PE updates the predicted resources with the latest telemetry values and sets the initial values of the resources for that given point in time (step 22).

Finally, the PE module sends the scheduling request to the scheduler module and receives an optimized schedule (steps 23-25). To close the circle, the PE updates the schedule and telemetry databases with the resulting schedule and predicted resources (steps 26-27). The obtained optimized schedule is then prepared to be distributed to the corresponding agents like satellite operators and GSN operators (step 28).

V. VALIDATION SCENARIO

This section proposed a scenario to validate the dynamic execution of the CMS. This constellation consists of a Walker star pattern with four polar planes and 16 satellites, 90°:16/4/1 in Walker notation. The scenario GSN, composed of AWS and KSAT, is shown in Table I. Regarding the traffic demand, twelve different SA have been defined. Six are in Europe: Spain, France, Germany, the Baltic, Italy, and the UK. The other six are in the USA: Florida, Washington, Dallas, Minnesota, Portland, and Las Vegas. These twelve regions are assumed to follow the same traffic model. The task types modeled for this simulation are Mobile Originated Upload (MOUL), Mobile Originated Download (MODL), Mobile Terminated Upload (MTUL), and Mobile Terminated Download (MTDL). Mobile Originated (MO) traffic is the one originated in the User Equipment (UE) and towards the IoT server, and Mobile Terminated (MT) traffic the other way around. The traffic model assumes that each service area generates 3.8 KB of data every three hours, which corresponds to the modeled memory cost of a single MOUL task. Likewise, the same amount of data generation is assumed from the IoT server to the service areas, corresponding to a single MTUL task.

TABLE I
SCENARIO GROUND SEGMENT

Name	Latitude (°)	Longitude (°)
AWS Punta Arenas	-52.93	-70.85
AWS Sydney	-33.74	151.18
AWS CapeTown	-33.95	18.43
KSAT Tromso	69.66	18.94
KSAT Inuvik	68.32	-133.61

For this validation, two different tests are conducted within the same time frame, one with open-loop optimization and another with a dynamic closed-loop optimization. The telemetry

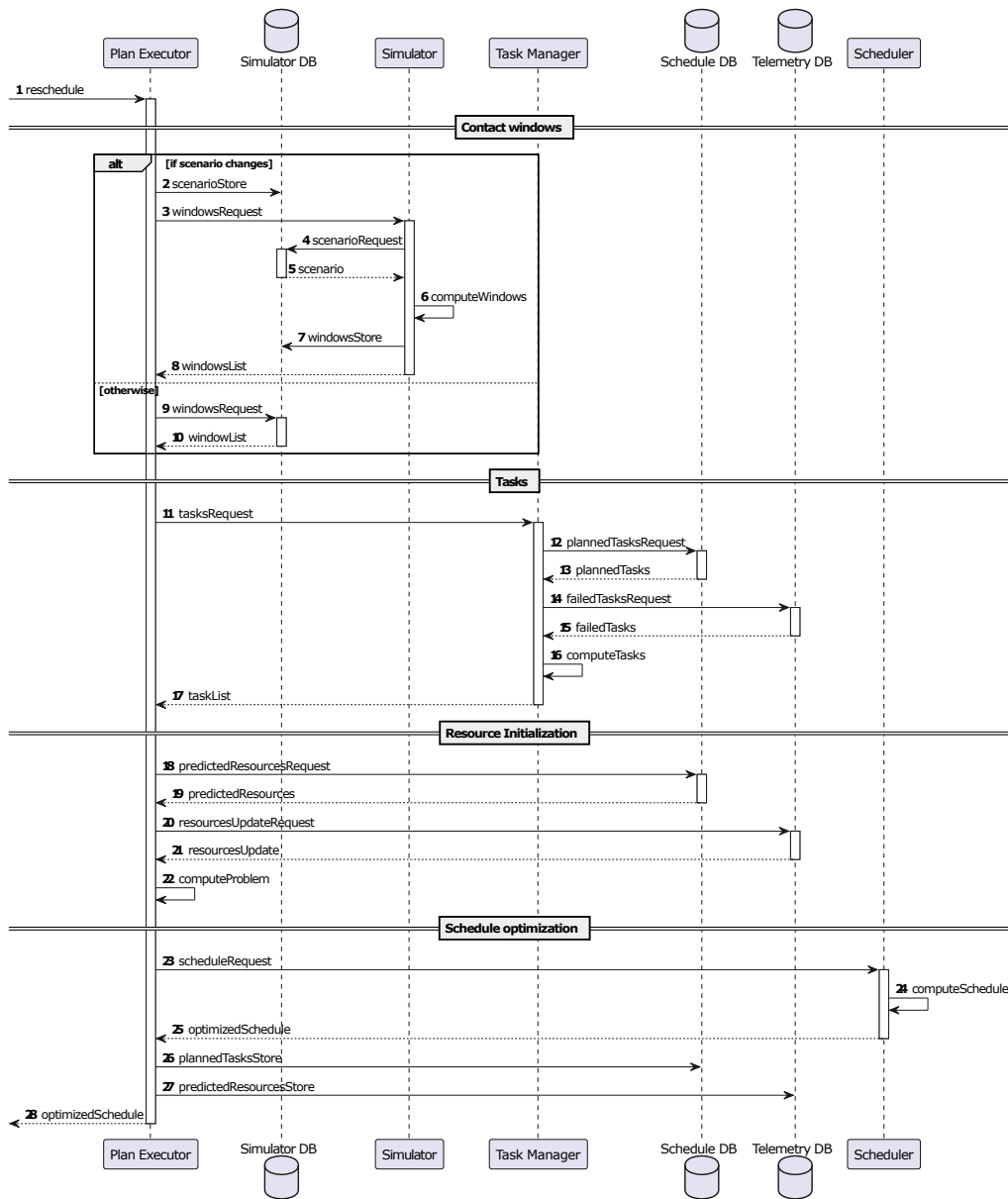


Figure 2. Sequence diagram of the CMS dynamic execution.

database does not contain any failed tasks at the beginning of the tests. Likewise, the schedule database is empty. After that, the PE is manually triggered to start, and approximately two hours later, new telemetry is added to the telemetry database. The telemetry will consist on new predefined resource levels for each satellite (within satellite resource boundaries), and a batch of failed tasks corresponding to the first 30 tasks of the original schedule, obtained two hours ago. In the closed-loop approach, the PE launches a reschedule every three hours with a time horizon of six hours. Therefore, an hour later to the telemetry input, a rescheduled request is automatically sent to the PE. For the open-loop test, the PE launches a reschedule at the end of the preceding schedule, in this case, every six hours. Figures 3 and 4 summarize the different test timelines

using relative minutes. These tests aim to validate that the telemetry is correctly read and its changes are autonomously introduced in future schedules, both for the satellite resources and the failed tasks. Moreover, the open-loop test provides a fundamental reference point against which to assess the benefits of employing a closed-loop approach. Additional information on the software used in the simulations can be found in [16] and [23].

VI. RESULTS

The results obtained from the test show that the telemetry feedback is correctly incorporated into the next autonomous operations schedule. Starting with the initial task list generated by the TM, Table II summarizes the number of tasks coming

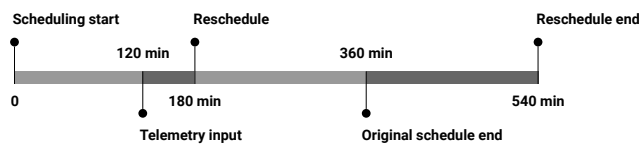


Figure 3. Closed-loop scheduling test timeline.

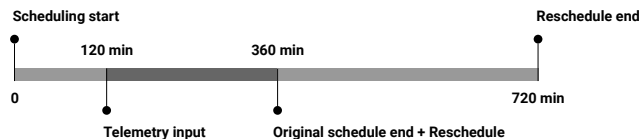


Figure 4. Open-loop scheduling test timeline.

from three different origins: (1) remaining tasks assigned in the last schedule, (2) failed tasks fetched from the telemetry database, and (3) the projected tasks until the end of the current schedule time horizon following the scenario traffic model. As can be seen, the starting schedule is not based on a past schedule. Therefore, no assigned tasks are still to be performed in the schedule database, nor any failed task in the telemetry database. Following the traffic model described in V and given that the total active SA is 12, the initial task list consists of only 96 tasks generated according to the traffic model. That is two MOUL and two MTUL tasks for each of the 12 SA and the same number of download tasks, a total of 8 tasks per SA. The automatic reschedule generated after three hours shows that it now consists of 129 tasks, divided into 51 remaining tasks from the original schedule, 30 failed tasks corresponding to the 30 first tasks of the original schedule, and 48 new tasks according to the traffic model. As can be seen, the TM has successfully fetched the original schedule and kept the assigned future tasks. It has also introduced the 30 tasks marked as failed in the telemetry database. Lastly, it has correctly computed the new projected tasks according to the traffic model, considering there are only three new hours to consider when generating new tasks. This yields one task of each type per SA, totaling 48.

The table also presents the mean throughput obtained in each schedule and for two different tests. The open-loop test serves as the baseline, and it involves initiating the rescheduling process after the preceding schedule time horizon, regardless of any telemetry alterations. As can be seen, the throughput obtained when using the close-loop approach explained in Section V increases by more than 10%. It is worth mentioning that in both schedules and tests, the scheduler assigned almost 100% of the initial tasks. This is because the scenario parameters allow an unconstrained scenario since this study focuses on dynamic scheduling rather than scheduler performance.

The other telemetry input that this dynamic scheduler integrates is the satellite resources. Figures 5 and 6 show a scenario of the satellite's memory and energy levels throughout the scheduling timespan. Three different plots are displayed:

 TABLE II
 TASK REASSIGNMENT RESULTS

	Original schedule	Reschedule
Remaining tasks	0	51
Failed tasks	0	30
Traffic model tasks	96	48
Total tasks	96	129
Schedule throughput (KB/h)	18.46	35.46
Open-loop test throughput (KB/h)	26.96	
Closed-loop test throughput (KB/h)	29.77	

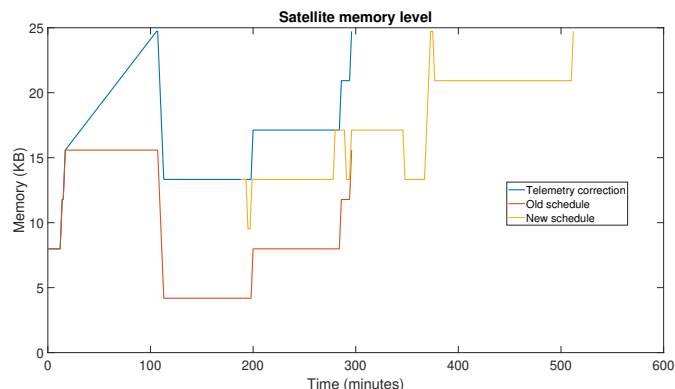


Figure 5. Satellite memory levels.

one for the propagated resources of the original schedule (old schedule in the figure legend), one for the telemetry correction on the propagated resources (telemetry correction in the figure legend), and another for the propagated resources of the reschedule (new schedule in the figure legend). As seen in both plots, the old schedule propagated resources and the ones corrected with the telemetry share the same pattern but diverge two hours into the propagation since this was when the telemetry was manually introduced to the database. It can also be observed that the new schedule starts from the telemetry-corrected levels of each resource. It is also worth mentioning that the new schedule is quite different from the old one since random telemetry values are added to each satellite, and 30 failed tasks have to be reassigned as well. Therefore, the scheduler has redistributed the tasks among all the 16 satellites of the constellation accordingly.

VII. CONCLUSION

This paper is a step forward in tackling the challenge of enhancing the robustness of the CMS, bringing it closer to the integration of network operations and satellite operations in 3GPP NTN. This work delves into the implementation of closed-loop operations management within the CMS framework, aiming to mitigate disruptions stemming from deviations in operational scheduling. This work presents an architecture enabling the autonomous integration of telemetry feedback and a sequence diagram outlining the rescheduling process. The outcomes of a case study underscore the necessity for dynamic scheduling and its potential advantages. The findings illustrate the system's ability to swiftly react, often within minutes, to

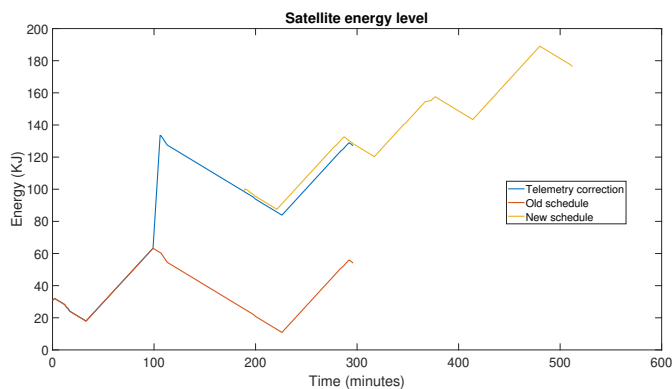


Figure 6. Satellite energy levels.

significant fluctuations in telemetry data, effectively managing variations in satellite resource levels and addressing task failures. Preliminary results have shown to improve throughput by 10% when using a closed-loop approach over an open-loop approach. Future research aims to optimize the timing of rescheduling, considering factors, such as scenario reactivity, telemetry fluctuations, and scheduling efficiency, among others. This research marks a significant step in enhancing the robustness and adaptability of centralized satellite constellation operations management in the face of dynamic and changing scenarios.

ACKNOWLEDGMENT

This work has been funded by the Government of Catalonia in the scope of the NewSpace Strategy for Catalonia. Additionally, this work was funded by the Spanish Ministry of Economic Affairs and Digital Transformation and the European Union – NextGeneration EU, in the framework of the Recovery Plan, Transformation and Resilience (PRTR) (Call UNICO I+D 5G 2021, ref. number TSI-063000-2021-1-6GSatNet-GS). This research was funded in part by the Spanish MCIN/AEI/ 10.13039/501100011033 through project PID2019-106808RA-I00, and by Secretaria d'Universitats i Recerca del departament d'Empresa i Coneixement de la Generalitat de Catalunya with the grant number 2021 SGR 00330. This paper is also part of the Grant 6G-DIFERENTE (CER-20231018) funded by CDTI and by the European Union NextGenerationEU/PRTR within the call "Ayudas Cervera para Centros Tecnológicos 2023. The research was partially supported by the Embry-Riddle Aeronautical University Faculty Research Development Program and GAANN fellowship.

REFERENCES

- [1] O. Kodheli, E. Lagunas, N. Maturo, S. K. Sharma, B. Shankar, J. F. M. Montoya, J. C. M. Duncan, D. Spano, S. Chatzinotas, S. Kisseleff, J. Querol, L. Lei, T. X. Vu, and G. Goussetis, "Satellite Communications in the New Space Era: A Survey and Future Challenges," *IEEE Communications Surveys & Tutorials*, vol. 23, no. 1, pp. 70–109, 2021.
- [2] J. A. R. de Azua, A. Calveras, and A. Camps, "Internet of Satellites (IoSat): Analysis of Network Models and Routing Protocol Requirements," *IEEE Access*, vol. 6, pp. 20 390–20 411, 2018.
- [3] M. M. Azari, S. Solanki, S. Chatzinotas, O. Kodheli, H. Sallouha, A. Colpaert, J. F. M. Montoya, S. Pollin, A. Haqiqatnejad, A. Mostaani, E. Lagunas, and B. Ottersten, "Evolution of Non-Terrestrial Networks From 5G to 6G: A Survey," *arXiv preprint arXiv:2107.06881*, 2021.
- [4] S. Wang and Q. Li, "Satellite Computing: Vision and Challenges," *IEEE Internet of Things Journal*, vol. 10, no. 24, pp. 22 514–22 529, Dec. 2023.
- [5] J. A. Fraire, O. Iova, and F. Valois, "Space-Terrestrial Integrated Internet of Things: Challenges and Opportunities," *IEEE Communications Magazine*, vol. 60, no. 12, pp. 64–70, dec 2022.
- [6] M. Harounabadi and T. Heyn, "Toward Integration of 6G-NTN to Terrestrial Mobile Networks: Research and Standardization Aspects," *IEEE Wireless Communications*, vol. 30, no. 6, pp. 20–26, Dec. 2023.
- [7] M. Marchese, F. Patrone, and A. Guidotti, *The Role of Satellite in 5G and Beyond*. Cham: Springer International Publishing, 2023, pp. 41–66. [Online]. Available: https://doi.org/10.1007/978-3-031-30762-1_2
- [8] 3rd Generation Partnership Project, "Study on architecture aspects for using satellite access in 5G (TR 23.737 Release 17)," Technical Specification Group, Tech. Rep., 2021.
- [9] —, "Solutions for NR to support non-terrestrial networks (NTN) (TR 23.737 Release 17)," Technical Specification Group, Tech. Rep., 2023.
- [10] —, "RadioAccess Network: Study on Narrow-Band Internet of Things (NB-IoT)/ Enhanced Machine Type Communication (eMTC) Support for Non-Terrestrial Networks (NTN) (Release 17)," Technical Specification Group, Tech. Rep., 2022.
- [11] M. Luglio, M. Quadrini, C. Roseti, and F. Zampognaro, "Scenarios and implementation use-cases for satellite-based NB-IoT," in *2021 International Symposium on Networks, Computers and Communications (ISNCC)*. IEEE, Oct. 2021.
- [12] R. B. Sørensen, H. K. Møller, and P. Koch, "5G NB-IoT via low density LEO Constellations," in *Small Satellite Conference*. arXiv, 2021.
- [13] E. Berrane and J. Soloff, *Designing Delay-Tolerant Applications for Store-and-Forward Networks*. Artech House, 2020.
- [14] T. Kellermann, R. P. Centelles, D. Camps-Mur, R. Ferrus, M. Guadalupi, and A. C. Auge, "Novel Architecture for Cellular IoT in Future Non-Terrestrial Networks: Store and Forward Adaptations for Enabling Discontinuous Feeder Link Operation," *IEEE Access*, vol. 10, pp. 68 922–68 936, 2022.
- [15] W. Yang, L. He, X. Liu, and Y. Chen, "Onboard coordination and scheduling of multiple autonomous satellites in an uncertain environment," *Advances in Space Research*, vol. 68, no. 11, pp. 4505–4524, Dec. 2021.
- [16] A. Singla, F. Criscola, E. Ponce, D. Canales, A. Calveras, and J. A. Ruiz-De-Azua, "Towards 6G Non-Terrestrial Networks - An Autonomous Constellation Management Engine," 2022, 33rd AAS/AIAA conference. Pending proceedings. [Online]. Available: https://www.researchgate.net/publication/369541726_Towards_6G_Non-Terrestrial_Networks_-_An_Autonomous_Constellation_Management_Engine
- [17] A. Iqbal, M.-L. Tham, Y. J. Wong, A. Al-Habashna, G. Wainer, Y. X. Zhu, and T. Dagiuklas, "Empowering Non-Terrestrial Networks With Artificial Intelligence: A Survey," *IEEE Access*, vol. 11, pp. 100 986–101 006, 2023.
- [18] Q. Chen, Y. Zhang, J. Guo, L. Yang, C. Fan, Y. Zhao, and X. Chen, "Traffic Prediction Based on Surrogate Model in Satellite Constellation Networks," in *2019 12th IFIP Wireless and Mobile Networking Conference (WMNC)*. IEEE, Sep. 2019.
- [19] M. Lopez-Benitez, C. Majumdar, and S. N. Merchant, "Aggregated Traffic Models for Real-World Data in the Internet of Things," *IEEE Wireless Communications Letters*, pp. 1–1, 2020.
- [20] R. D. McAllister, J. B. Rawlings, and C. T. Maravelias, "The inherent robustness of closed-loop scheduling," *Computers & Chemical Engineering*, vol. 159, p. 107678, Mar. 2022.
- [21] G. Stock, J. A. Fraire, T. Mömke, H. Hermanns, F. Babayev, and E. Cruz, "Managing fleets of LEO satellites: Nonlinear, optimal, efficient, scalable, usable, and robust," *IEEE Transactions on Computer-Aided Design of Integrated Circuits and Systems*, vol. 39, no. 11, pp. 3762–3773, 2020.
- [22] G. Stock, J. A. Fraire, H. Hermanns, E. Cruz, A. Isaacs, and Z. Imbrosh, "On the automation, optimization, and in-orbit validation of intelligent satellite constellation operations," 2022.
- [23] A. Singla, A. Calveras, F. Betorz, and J. A. Ruiz-De-Azua, "Enhancing Satellite Non-Terrestrial Networks Through Advanced Constellation Management: Optimizing In-Orbit Resources for NB-IoT," *IEEE Open Journal of the Communications Society*, vol. 5, pp. 2113–2131, 2024.

Enhanced Path Reliability of Contact Graph Routing through a Cognitive Extension

Ricardo Lent
 Engineering Technology
 University of Houston
 Houston, Texas, USA
 rlent@uh.edu

Abstract—Delay-Tolerant Networking allows forwarding data bundles over space networks whose dynamics create a disconnected state for extended periods. Routing in such an environment is challenging and central for effective end-to-end data delivery. In this study, we enhance the routing accuracy Contact Graph Routing (CGR) by introducing a Cognitive Element (CE). The core idea revolves around establishing a data-driven methodology where the CE uses regression based on selected inputs to estimate the average single-hop bundle delivery time. This estimation is then integrated into the time progression step of CGR's shortest-path algorithm. By doing so, one-hop bundle times can be accurately predicted, taking into account various factors such as, specific Convergence Layer Adapter (CLA) behavior, configuration parameters, and random factors like the probability of packet drops and the use of unreliable contacts. The end result is a performance enhancement for bundle paths. The paper evaluates the idea from an implementation-agnostic perspective, assessing the performance advantages of using the CE with CGR. Additionally, the study assesses the potential performance degradation associated with reduced prediction accuracy, which may arise due to partial data or limitations of the regression model. The evaluation is carried out using a simulated Earth-Moon network context, with realistic values for contact features and considering unreliable contacts. The study provides insights into the practical implications of the proposed approach.

Keywords—delay-tolerant networking; routing; reliability; performance evaluation; cognitive networking

I. INTRODUCTION

Space Delay-Tolerant Networks (DTNs) are crucial in facilitating communication among spacecraft, rovers, orbiters, landers, and ground stations in space exploration missions that often times involve significant signal propagation delays because of the long-distance communication links and periods of signal disruption due to celestial bodies obstructing line-of-sight communication paths and other factors. Routing is a key component of space DTNs that determines the store-carry-and-forward communication path for data bundles. The pre-planned nature of these networks simplifies the routing task, as contact opportunities can be anticipated from the expected positions of nodes as derived from orbital calculations. These calculations not only identify link obstructions but also provide the information required for a link budget analysis. Contact Graph Routing (CGR) leverages the contact information to distributively compute the optimal next-hop for bundles achieving data forwarding efficiency.

This work was supported by grant #80NSSC22K0259 from the National Aeronautics and Space Administration (NASA).

However, it is relevant to point out that, despite the deterministic assumption of contacts in scheduled DTNs, variations can still arise due to a multitude of factors. For instance, cloud coverage can bring large signal attenuation at high radio frequencies and in free-space optical links that can disrupt expected contacts between an orbiter and a ground node. Node malfunction and antenna misalignment issues may also occur randomly preventing contact realizations. Moreover, operational priorities may dynamically change resulting in the re-assignment of expected contacts to a different application. These observations are aligned with the evolution of Opportunistic Contact Graph Routing (OCGR) [1], which explores the potential utilization of non-scheduled contacts associated with a calculated confidence level. OCGR introduces a shift in the path search methodology of CGR, allowing the discovery of the k -shortest paths and the assessment of path reliability. Extending this concept further, it can be assumed that all contacts in a DTN have an opportunistic nature, including scheduled contacts, as they may randomly fail as discussed. Therefore, at least the path searching part of OCGR can be widely applicable to optimize unreliable DTN scenarios, provided each contact can be associated with a confidence level.

One limitation of CGR (and OCGR) is that the time progression step of each bundle forwarding within the path search algorithm assumes ideal transmission conditions. Buffering information is considered unavailable beyond the links leading to neighboring nodes, therefore not fully accounting for queuing delays. Additionally, protocol dynamics, including the convergence-layer adapter (CLA), particularly concerning the handling of packet losses through retransmissions, are largely overlooked. These factors contribute to differences between the calculated times within the CGR path search algorithm and the actual bundle forwarding performance, potentially impacting routing optimally.

In this paper, we explore the integration of a Cognitive Element (CE) into CGR to enhance routing performance. The fundamental idea is that the CE can generate accurate one-hop bundle time calculations, aiding the CGR shortest-time algorithm in identifying the best paths after considering their realistic performance. The main contributions of this work include:

- 1) The concept of a CE to forecast the average single-hop bundle delivery time to be used in the time progression step of CGR. The core idea is to introduce a data-driven approach that will help identifying the best path

considering factors that include specific Convergence-Layer Adapted (CLA) behavior and its configuration parameters, as well as random factors, such as packet drops and the use of unreliable contacts. Since the approach is data-driven, the CE could be trained either offline using an analytical model or historical data, or progressively online with real measurements to achieve accurate predictions. This approach eliminates the need for modifications to the CGR algorithm to account for uncertain contacts and other random factors. Thus, it removes the need for searching for the k -shortest paths, as implemented in OCGR.

- 2) An evaluation of the performance impact of the limitations of the CE in producing accurate bundle time estimations. The CE provides a function that maps the known network state to forecast the time required for a bundle to reach the next hop. The limitations of the method are therefore related to the accuracy of the network state knowledge, particularly because the required information may not necessarily be available at the nodes. This study provides an implementation-agnostic assessment of the performance advantages and limitations of the CE, identifying the performance bounds of the method across two variations regarding the severity of assumptions involving the network state. In the first case, only local state information, which is normally available to standard CGR, is assumed. The second case requires global knowledge, i.e., information external to the node, and gives the best case scenario. The evaluation is conducted within the context of an Earth-Moon network [2], employing approximately realistic values for contact features and considering unreliable contacts. The evaluation provides insight into the impact of imperfect CE model predictions on end-to-end bundle routing performance.

The remainder of the paper is structured as follows: Section II offers a summary of related works pertinent to this study. Section III elaborates on the CE method. Section IV discusses the evaluation scenario and simulation assumptions. Section V presents the results showing the application of the CE in optimizing bundle flow over an Earth-Moon network. Lastly, concluding remarks are provided in Section VI.

II. RELATED WORKS

The reliability of DTN protocols remains a dynamic area of research with application to many ambitious missions [2]. A feature that characterizes space DTNs is the use of scheduled contacts, commonly used jointly with the Bundle Protocol (BP) [3], [4] and Contact Graph Routing (CGR) [5], which begins by constructing a graph, where vertices denote active contacts and links represent logical transitions between contacts—where one contact’s endpoint aligns with the next contact’s starting point, feasible within a defined time frame. While this process incorporates factors, such as transmission time, propagation delay, and network disruptions, buffering

delays are typically overlooked due to the distributed nature of the algorithm, as this information is normally inaccessible.

The performance of CGR in scenarios involving unreliable links has been explored in various contexts, including satellite constellations [6] and random networks [7]. Reliability has been mainly addressed by BP custody [8] and CLA design via retransmissions, e.g., the Licklider Transmission Protocol (LTP). For experimental results, see for example [9]–[11]. These studies have shed light on CGR’s vulnerabilities concerning contact failure rates and random losses. An extension known as Opportunistic CGR (OCGR) investigates the potential integration of nonscheduled contacts—either discovered or predicted—into CGR’s standard path search algorithm, assigning them a confidence level. OCGR maintains a record of the contact history of nonscheduled contacts to predict future contacts, alongside their associated properties and confidence levels, calculated based on available contact history [1]. Discovered contacts are assigned a unit confidence [12] and the resulting route is assigned a delivery confidence derived from the product of the confidence levels of the contacts involved. In recent iterations, the implementation of OCGR [13] evaluates path candidates based on their arrival confidence, considering a predefined margin from the highest confidence level.

Additional related methods to this work include Roaming DTN (RDTN) [14] that integrates roaming nodes with unpredictable motion, Best Routing Under Failures (BRUF) [15], where the routing process is conceptualized as a Markov Decision Process, with certain state transitions becoming probabilistic due to the limited reliability of specific contacts and Routing under Uncertain Contact Plans (RUCoP) [16], [17] that introduces a multiple-copy Markov Decision Process. Also related, is the Cognitive Space Gateway (CSG) [18] where routing decisions are delegated to a Spiking Neural Network which is continually trained after the bundle transmissions using a reinforcement learning approach.

This paper presents an alternative approach to enhance CGR performance, a method known for its computational efficiency and practicality, but limited in handling random factors impacting single-hop bundle transmissions, such as packet losses and contact failures. Unlike previous approaches, this method modifies the conventional one-hop bundle time calculations. Specifically, it introduces the idea of using a cognitive element designed to accurately predict average bundle transmission times. While the implementation of this cognitive element is expected to utilize a neural network or similar structure, this study evaluates its limitations without specifying a particular technology. Instead, it offers widely applicable findings focused on determining performance bounds based on assumptions regarding available network state information used as inputs to the CE.

III. COGNITIVE EXTENSION AND CGR

CGR uses a decentralized approach where the next hop is calculated as soon as a bundle is received by each DTN node on the path by recomputing the best route to destination.

A. Standard Mechanisms

The method requires knowledge of the network contact plan listing all future contacts, which is distributed to the DTN nodes in advance. The i -th entry in the contact plan is the tuple $(\mathcal{I}_i, \mathcal{F}_i, \mathcal{T}_i, \mathcal{S}_i, \mathcal{E}_i, \mathcal{R}_i, \mathcal{O}_i, r_i)$ that includes a contact identifier \mathcal{I}_i , the sending \mathcal{F}_i and receiving node \mathcal{T}_i identifiers, the start \mathcal{S}_i and end \mathcal{E}_i times the transmission rate \mathcal{R}_i and the propagation delay or one-way light time \mathcal{O}_i that depends on the distance between the nodes. The term r_i , $0 \leq r_i \leq 1$, is the contact confidence OCGR [1].

To determine routing for each desired destination, CGR builds a contact graph $G = (V, E)$ using each contact entry in the plan as a vertex minus the entries containing excluded nodes (e.g., known failed nodes). A contact graph is a directed acyclic graph whose edges represent the time periods of forced data buffering due to the corresponding link disruption. An edge exists when two contacts are logically connected, which happens when the destination node of the first contact matches the sending node of the second contact and the latter expires after the first. The target contact of an edge is called the proximate of the first contact. CGR derives the next hop for the bundle from the shortest path on the contact graph between two auxiliary vertices that represent the root and terminal contacts. These auxiliary contacts involve a zero-cost contact between the current DTN node and the destination node to themselves. Starting from the root, a graph traversal based on Dijkstra's algorithm iteratively tracks the bundle transmission progress in the network by estimating its arrival time as it is forwarded over contacts that are logically connected. That is, if t_i represents the bundle arrival time calculated at vertex i , the algorithm evaluates the proximate vertices j and greedily chooses the one offering the smallest t_j . Specifically, the evaluation of the proximate vertex j , yields the following arrival time.

$$t_j = \begin{cases} t_i + \mathcal{O}_j & \mathcal{S}_i \leq t_i \\ \mathcal{S}_j + \mathcal{O}_j & \mathcal{S}_i > t_i \end{cases} \quad (1)$$

The calculation does not include transmission time, but that metric is utilized to determine the remaining data volume for transmissions. This additional step enables the consideration of whether given contacts are likely to be already fully booked. However, this assessment is restricted to contacts leading to neighboring nodes, as information beyond that scope is unavailable. The output of the algorithm is the path $P = v_0, v_1, \dots, v_k$, where $v_i \in V$ is a contact and v_0, v_k are the auxiliary contact entries for the source and sink nodes respectively. If t_k is the estimated time to deliver the bundle to the end contact based on (1) for each step, the objective of the algorithm is to minimize t_k among all possible paths from v_0 to v_k in G .

B. Cognitive Element

The central idea of this paper is to enhance the route selection quality in CGR by refining the accuracy of the single-step bundle forwarding time calculation. This involves substituting the computation outlined in (1) with the output

of a cognitive element (CE) designed to accurately predict the time needed to deliver a bundle to the next hop, accounting for the segmentation, transmission and retransmission times of the convergence-layer adapter, buffering delays, and the reliability of contacts, among other factors:

$$t_j = t_i + y_j \quad (2)$$

where $y_j = f_\theta(x)$ represents the output of a regression function f_θ given the specified system state x and the model parameters θ .

A second modification concerns the interpretation of t_j , which now represents the average time to reach the next hop, rather than the precise definition in CGR. This change is required to properly take into account probabilistic factors, such as transmission errors and contact failures. The idea is that these probabilistic factors will affect the one-hop bundle delivery time along the path adding uncertainty into the calculation of the final delivery time. With this reinterpretation of t_j , the shortest path algorithm of CGR requires no modification. It continues to identify the route with the smallest average time of arrival t_k (instead of precise time), but now able to accommodate random factors affecting the paths.

In this study, we keep the concept of introducing a CE to CGR separated from its implementation on purpose, recognizing that diverse techniques may be used to define this element. Possible mechanisms encompass a range of neural network architectures, including multi-layer feedforward, convolutional, generative adversarial, recurrent (such as Long Short-Term Memory Networks), autoencoders, graph neural networks, and more. These mechanisms can be implemented using either continuous activation or spiking neurons. Given the potential variations in prediction accuracy resulting among different techniques, our focus is in assessing the performance bounds attained with the introduction of the CE concept and understanding the performance implications of imperfect prediction accuracy by $f_\theta(x)$. In particular, we focus on studying two variations for $f_\theta(x)$. The first case, which is labeled CE-A, considers $f_\theta(x)$ providing an estimation of the average one-hop bundle time that aggregates the bundle transmission time, propagation delay, and contact reliability. The latter factor probabilistically extends the one-hop bundle time when one or more contacts to the neighbor node fail. The second case, CE-B, considers all factors of the former case but adds buffering times.

Regarding the training of the models, it is worth noting that CE-A is comparatively easier to train since it only requires local state information, such as the parameters available in the contact plan: transmission rate, propagation delay, and confidence level (an estimation of contact reliability). CE-B requires predicting the global state, as the buffer occupancy levels are dynamic. To maintain the study's focus on evaluating the effectiveness of the CE concept rather than discussing specific approaches, we omit further details of the training phase for these models.

IV. EVALUATION SCENARIO

To evaluate the advantages and limitations of the CE in improving CGR optimality, we consider an Earth-Moon communication scenario where data periodically collected by a rover on the Moon must be delivered to a terrestrial sink. The focus is on observing the time required to deliver the data with and without the CE extension, and on assessing the impact of the network state knowledge used by the CE. To this end, two simulators were developed. The first simulator generates the contact plan by estimating the locations of nodes using orbital calculations and accounting for both Earth's and Moon's rotation and translation, which helps determine transmission opportunities in the scenario. The second simulator evaluates routing performance through event-driven simulations of bundle transmissions and buffering, with considerations for potential contact failures.

In the simulation, the traffic originates from a Lunar rover positioned on the far side of the Moon, with three orbital relays available to forward the data to Earth: LO1, LO2, and LO3. For simplicity, Keplerian orbits were used and the contact opportunities were determined solely by line-of-sight considerations. These orbits are characterized by inclinations of 10, 40, and -40 degrees, and Right Ascension of the Ascending Node (RAAN) values of 4.462, 90, and 40 respectively. It is relevant to emphasize that these orbits are not representative of existing lunar satellites but were defined to facilitate the establishment of contacts of varying durations with the rover and the Earth stations.

The terrestrial ground stations are modeled to match with the locations of the Deep-Space Communication (DSN) complexes in Canberra, Madrid, and Goldstone. The sink is assumed to be situated in Houston, with a permanent link established from each DSN location to Houston. Propagation delays for the contacts were determined based on the distance between the nodes involved and for the terrestrial links, i.e., from each of the DSN nodes to the Houston node, the propagation delay was calculated based on the as-the-crow-flies distance plus a 20% margin to accommodate cable routing overhead. Table I provides the average and standard deviation of the contact characteristics between the rover and the lunar orbiters, as well as between the lunar orbiters and the terrestrial stations

The transmission rate for the terrestrial (wired) links was fixed to 2 Mbps whereas all wireless transmissions were set to 100 Kbps. In all cases, the links are also assumed to be affected by negligible bit error rates (BER). Also, it is assumed that all contacts are reliable except for the orbiter to ground station links given the long distance involved. In particular, one link is assumed to be severed affected. The reliability of the links originated at each orbiter were set to 0.95, 0.85, and 0.5 respectively. In this context, CGR defines for each generated bundle by the rover which orbiter will handle the bundle forwarding to Earth and which ground station will receive the bundle before forwarding it to the sink. Bundles are not associated with a finite deadline and the DTN buffers are

TABLE I. AVERAGE (μ) AND STANDARD DEVIATION (σ) OF CONTACT DURATIONS AND PERIOD LENGTHS (TIME BETWEEN CONSECUTIVE CONTACTS) FOR THE EARTH-MOON EVALUATION NETWORK.

Contact type	Duration μ	Duration σ	Period μ	Period σ
Rover to LO1	13.0	1.9	91.4	3.4
Rover to LO2	10.4	3.8	90.6	10.3
Rover to LO3	13.3	2.5	91.1	6.5
LO1 to Madrid	55.0	10.8	149.7	186.7
LO1 to Canberra	53.7	12.8	160.9	217.7
LO1 to Goldstone	55.3	9.5	147.1	185.2
LO2 to Madrid	56.7	19.0	147.5	181.6
LO2 to Canberra	61.2	12.0	170.4	229.9
LO2 to Goldstone	58.9	16.6	147.9	189.4
LO3 to Madrid	69.8	15.1	152.3	196.4
LO3 to Canberra	75.7	67.4	178.6	239.4
LO3 to Goldstone	68.8	16.7	146.6	194.4

assumed to be large enough to ignore the impact of buffer overflows, so bundles that miss any given contact simply continue waiting in the buffer for future service.

V. RESULTS AND DISCUSSION

The routing performance of the CE for CGR is evaluated based on the average delivery time, which represents the average response time of the bundle flow. CE-based predictions are mathematically obtained from the defined inputs to ensure general applicability and independence from any specific regression method. This evaluation is conducted under simulation conditions where buffer capacities are uncapped, bit error rates (BER) are negligible, and no deadlines are imposed on bundle delivery times. With these conditions, the risk of bundle loss is minimal. Bundles are generated at a constant rate of one every 100 seconds, while the bundle size is varied as an experimental parameter to observe routing performance across different traffic load levels.

A. Impact of the Offered Load

Figure 1 depicts the average response time for bundles. The response time of a bundle is calculated as the difference between its arrival time at the sink and its generation time. This metric aggregates transmission times, buffering durations, and waiting periods for contacts along the selected path. The results show the 95% confidence interval of the acquired samples for each observation point. As depicted in Figure 1, the average time required to transmit small files is approximately one hour. This duration is primarily determined by the waiting times for the next contact opportunities, given that buffering and transmission times are negligible under light traffic conditions. Additionally, this times accounts for the impact of contact failures. With increasing file sizes, there is a corresponding rise in both storage and transmission demands, resulting in an increase in the average response time.

For baseline performance, A-CGR is CGR with the exclusion of contacts less reliable than a predetermined threshold. This threshold was set to 0.9. A-CGR is functionally similar to O-CGR but simpler to implement. It is worth noting that the exclusion of low-reliable contacts leads to a better response time compared to the conventional CGR approach for both

light and heavy traffic loads. The simulations suggest that the results may reverse for a range of offered loads where the additional capacity of the excluded contacts may contribute to better distribute the traffic load despite with low reliability. Both cognitive extensions for CGR offer significantly lower delay than CGR and A-CGR with a performance that is almost indistinguishable for light loads. Because CE-A does not predict the impact of the queuing delay, it produces degraded performance compared to CE-B as buffers start filling up with heavier traffic loads. This degradation becomes evident around 20 kB/s, as illustrated in Figure 1.

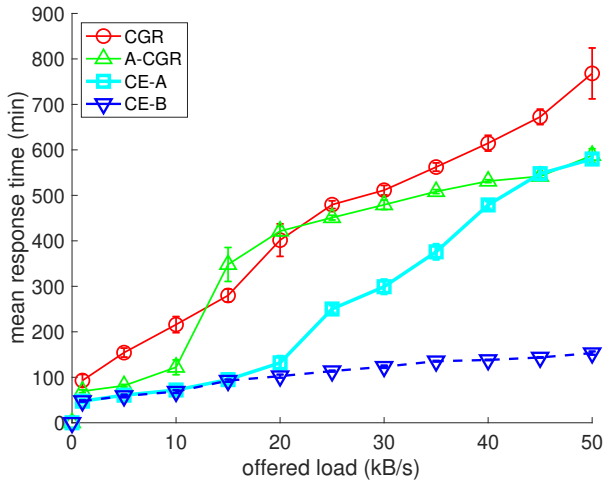


Figure 1. Average bundle delivery time as a function of the offered load.

B. Impact of the Prediction Error

A second set of experiments were run to quantify the impact of prediction errors in the cognitive methods to forecast bundle transmission times. To achieve control over the error level, deviations were introduced to the ideal prediction y as follows:

$$y' = \max\{y_{min}, y \times \mathcal{N}(1, \sigma_e)\} \quad (3)$$

where y_{min} is a lower threshold (0.1 in the tests) and $\mathcal{N}(1, \sigma_e)$ is a sample from a normal distribution with unit mean and standard deviation σ_e . The value y' is used in place of y in the shortest path algorithm when advancing the bundle progress time.

The value of σ_e in (3) is a controllable error factor in the experiments that models the accuracy of the cognitive unit in producing bundle transmission times predictions. Basically, it tells on average how many times smaller (if less than one) or larger (otherwise) the cognitive predictions are compared to the actual values.

Observations were collected for two reference traffic load points: 10 kB/s (Figure 2) and 30 kB/s (Figure 3). The results illustrate that small deviations in the predicted values from the actual values produce strong degradation with mean response times increasing sharply for error factors deviating the prediction approximately up to four times the actual values.

This observation is applicable to both cognitive prediction methods. With larger errors, the performance continues to degrade but at a smaller rate. Interestingly, an error factor of around 30 is required to make CE-A perform similarly to conventional CGR at either load level whereas CE-B was able to perform better than CGR regardless how large the error factor value.

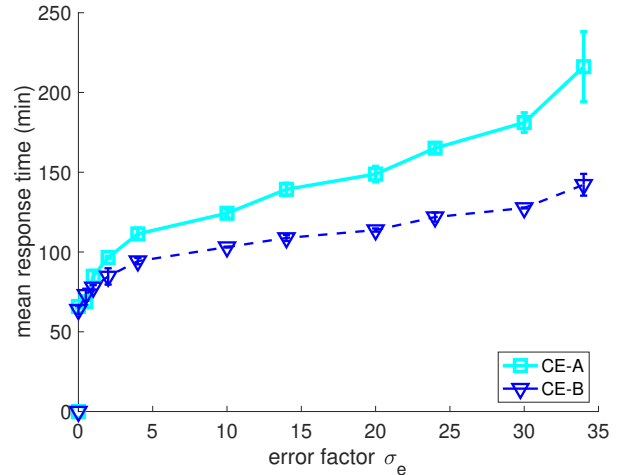


Figure 2. Impact of the prediction error σ_e for a traffic load of 10 kB/s.

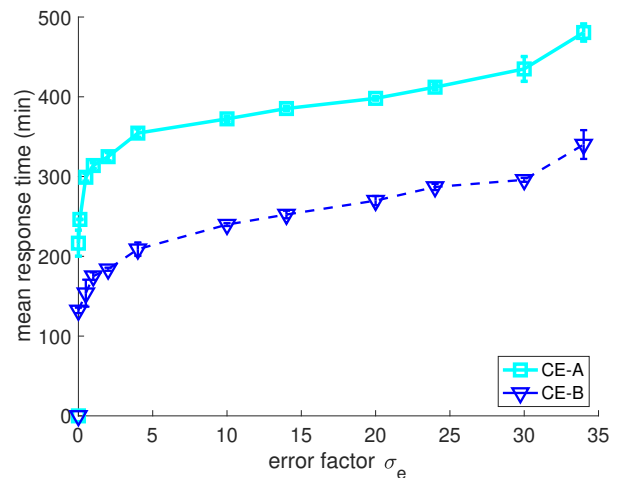


Figure 3. Impact of the prediction error σ_e for a traffic load of 30 kB/s.

VI. CONCLUSION

In conclusion, this study demonstrates the efficacy of integrating a cognitive element into CGR to enhance routing accuracy in a DTN. By leveraging a data-driven methodology, the CE aims to predict average single-hop bundle delivery times, considering various factors such as CLA protocol behavior (e.g., retransmission dynamics), configuration parameters, and random factors like packet drops and the presence of unreliable contacts.

Comprehensive simulations conducted within an Earth-Moon network simulated context, assuming realistic contact features and accounting for unreliable contacts, significant improvements in routing performance were observed with the CE compared to the conventional CGR approach. This was evident when considering both regular network information available at a DTN node, i.e., the information contained in the contact plan, and extending this information to include network-wide buffer occupancies, i.e., global information. Unsurprisingly, the latter assumption yielded the largest routing performance improvement, with average end-to-end times reduced by 2 to 4 times, particularly for traffic loads exceeding 20 kB in the tests, i.e., under congestion. However, even in the absence of global information, the CE achieved approximately 25 to 50% lower bundle delivery times on average compared to the standard CGR approach.

This study conducted an implementation-agnostic assessment of the proposed approach by using an analytic definition of the CE and the prediction errors. In practice, the CE is expected to be provided by a neural network or related mechanism, whose structure, training algorithm, and data availability and quality will determine its regression accuracy. The study highlights the likely performance degradation induced by such regression errors. Interestingly, the results suggest that the CE method is particularly sensitive to small errors. Notably, a Gaussian error with a standard deviation of 4 or less was found to double the average end-to-end delivery time for bundles, while larger errors had a comparatively smaller impact. These findings emphasize the benefits of employing a cognitive networking approach to optimize space DTN performance and the importance of designing an accurate CE. Future research is needed to develop the practical application of this concept.

REFERENCES

- [1] M. S. Net and S. Burleigh, "Evaluation of Opportunistic Contact Graph Routing in random mobility environments," in *2018 6th IEEE International Conference on Wireless for Space and Extreme Environments (WiSEE)*, pp. 183–188, Dec 2018.
- [2] D. J. Israel et al. "LunaNet: a flexible and extensible Lunar exploration communications and navigation infrastructure," in *2020 IEEE Aerospace Conference*, pp. 1–14, 2020.
- [3] K. Scott and S. C. Burleigh, "Bundle Protocol Specification," RFC 5050, Nov. 2007.
- [4] S. Burleigh, K. Fall, and E. J. Birrane, "Bundle Protocol Version 7," RFC 9171, Jan. 2022.
- [5] S. Burleigh, C. Caini, J. J. Messina, and M. Rodolfi, "Toward a unified routing framework for Delay-Tolerant Networking," in *2016 IEEE International Conference on Wireless for Space and Extreme Environments (WiSEE)*, pp. 82–86, 2016.
- [6] J. A. Fraire et al., "Assessing Contact Graph Routing performance and reliability in distributed satellite constellations," *J. Comput. Netw. Commun.*, vol. 2017, Jan 2017.
- [7] P. G. Madoery, F. D. Raverta, J. A. Fraire, and J. M. Finochietto, "Routing in space Delay Tolerant Networks under uncertain contact plans," in *2018 IEEE International Conference on Communications (ICC)*, pp. 1–6, 2018.
- [8] K. Zhao et al., "Performance of bundle Protocol for deep-space communications," *IEEE Transactions on Aerospace and Electronic Systems*, vol. 52, no. 5, pp. 2347–2361, 2016.
- [9] R. Wang et al., "A study of DTN for reliable data delivery from space station to ground station," *IEEE Journal on Selected Areas in Communications*, pp. 1–1, 2024.
- [10] C. Caini, T. de Cola, A. Shrestha, and A. Zappacosta, "LTP performance on near-Earth optical links," *IEEE Transactions on Aerospace and Electronic Systems*, vol. 59, no. 6, pp. 9501–9511, 2023.
- [11] J. Liang et al., "LTP for reliable data delivery from space station to ground station in the presence of link disruption," *IEEE Aerospace and Electronic Systems Magazine*, vol. 38, no. 9, pp. 24–33, 2023.
- [12] A. Berlati et al., "Implementation of (O-)CGR in The ONE," in *2017 6th International Conference on Space Mission Challenges for Information Technology (SMC-IT)*, pp. 132–135, 2017.
- [13] The Interplanetary Overlay Network (ION) software distribution, "ION-DTN," <https://sourceforge.net/projects/ion-dtn>. Retrieved: 05-01-2024.
- [14] D. Ta et al., "Roaming DTN: Integrating unscheduled nodes into contact plan based DTN networks," in *2023 IEEE Cognitive Communications for Aerospace Applications Workshop (CCA AW)*, pp. 1–9, 2023.
- [15] F. D. Raverta et al., "A Markov decision process for routing in space DTNs with uncertain contact plans," in *2018 6th IEEE International Conference on Wireless for Space and Extreme Environments (WiSEE)*, pp. 189–194, 2018.
- [16] F. D. Raverta et al., "Routing in Delay-Tolerant Networks under uncertain contact plans," *CoRR*, vol. abs/2108.07092, 2021.
- [17] P. R. D'Argenio, J. A. Fraire, A. Hartmanns, and F. Raverta, "Comparing statistical and analytical routing approaches for Delay-Tolerant Networks." Berlin, Heidelberg: Springer-Verlag, 2022.
- [18] R. Lent, "Implementing a cognitive routing method for High-Rate Delay Tolerant Networking," in *2023 IEEE Cognitive Communications for Aerospace Applications Workshop (CCA AW)*, pp. 1–6, 2023.

Spectral Target Detection at Twilight

Robert L. Sundberg
Spectral Sciences, Inc.
Burlington, MA, USA
e-mail: rob@spectral.com

Abstract— This paper will discuss the use of the Monte Carlo Scene (MCScene) code to simulate low light situations where the sun is near or below the horizon. MCScene is a high-fidelity model for full optical spectrum simulation. It provides an accurate, robust, and efficient means to generate spectral scenes for algorithm development and sensor trade studies. MCScene utilizes a Direct Simulation Monte Carlo (DSMC) approach for modeling 3D atmospheric radiative transfer including full treatment of molecular absorption and Rayleigh scattering, aerosol absorption and scattering, and multiple scattering. This paper will examine rare target detection statistics in simulated scenes as the sun moves from overhead to sunset and eventually to twilight.

Keywords— scene simulation; target detection; hyperspectral; multispectral

I. INTRODUCTION

Improved simulations of hyperspectral and multispectral imagery (HSI and MSI) under low illumination conditions are required to keep pace with the improved imaging capabilities of spectral imaging sensors, see for example imagery from BlackSky [1]. The MCScene code is a high-fidelity spectral image simulation capability [2], [3], that is based on a DSMC approach for modeling the 3D radiative transport. The code has been enhanced to allow treatment of long atmospheric path simulations such as those found under twilight conditions and highly off-nadir or near horizontal viewing geometries [4].

In this paper, we report on the initial results in a study on sub-pixel spectral target detection under low light conditions. Reflective boundary planes implemented in MCScene allows the code to simulate long path length scenes such as those encountered in limb viewing sensors or scenes where the sun is very low on the horizon or even below the horizon, twilight conditions. In Section II, we present some imagery simulated for three scene showing the low illumination simulations capabilities of MCScene. In Section III, we examined detection statistics for subpixel targets embedded in the simulated scenes as a function of solar zenith angle. Conclusions for the paper are presented in Section IV.

II. LOW ILLUMINATION SCENE SIMULATIONS

An example of low illumination simulation is shown in Figure 1. This figure shows a series of simulations for a sensor at 20 km altitude looking due west with a 45° slant angle as the sun sets over Fort Collins, CO. The simulation requires a reflectance map and a Digital Elevation Map

(DEM), we used a Landsat based reflectance map and downloaded the DEM from the USGS site [5]. A mid-latitude summer atmosphere was used along with a rural aerosol, as defined in MODTRAN [6]. The RGB bands of the simulation are shown for solar zenith angles of 30, 45, 60 and 70 degrees. Note the color change as the scene coloring shifts toward the red as the sun sets. When the sun is below the mountain peaks only photons which undergo multiple scattering can illuminate the shadowed ground.

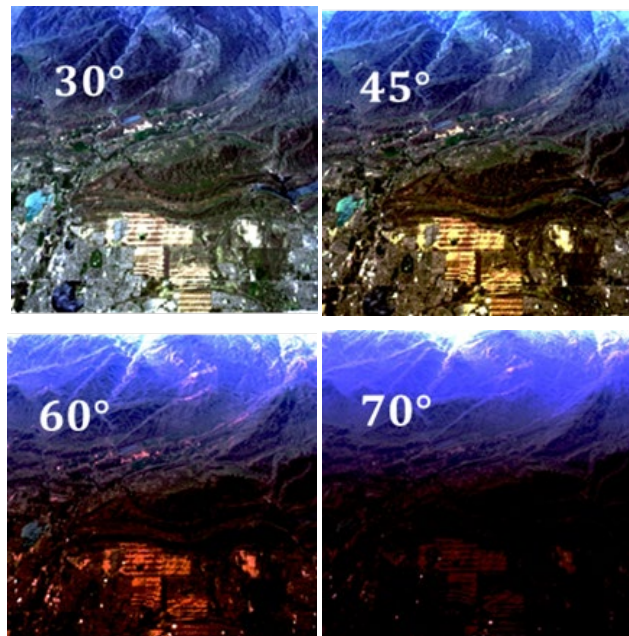


Figure 1. Linear stretched RGB radiance images simulated by MCScene for a Fort Collins, CO for solar zenith angles of 30, 45, 60 and 70 degrees.

In another example, a mountain ridge was used to cast a shadow over part of the Rochester Institute of Technology (RIT) Center for Imaging Sciences collected scene of Cook City, MT [7]. Figure 2 shows the RGB radiance images for a series of simulations with solar zenith angles of 0, 80, and 90 degrees. With a solar zenith angle of 80 degrees the scene is fully in shadow. The MCScene simulations were performed with an observer placed at 20 km altitude viewing nadir.

The final example shows a scene derived from a 1999 AVIRIS data collect over a Boreal region in Saskatchewan, Canada [8]. We have resampled the spectral imagery to match the 126 spectral bands of the HyMap sensor [9] to speed up the spectral simulations, which scale linearly with the number of spectral bands. Figure 3 shows a linear stretch of the RGB radiance images for a subset of the Boreal scene

for solar zenith angles of 45 and 90 degrees. These scenes were simulated for a sensor at 20 km altitude looking nadir with very low aerosol loading with a resulting visibility of 100 km. The image at 90-degrees solar zenith shows additional noise but much of the spectral content appears present even when the scene radiance is down by nearly four orders of magnitude.



Figure 2. Linear stretched RGB radiance images simulated by MCSScene for a subset of the RIT Target Detection Blind-Test scene for solar zenith angles of 0 (top), 80 and 90 (bottom) degrees.

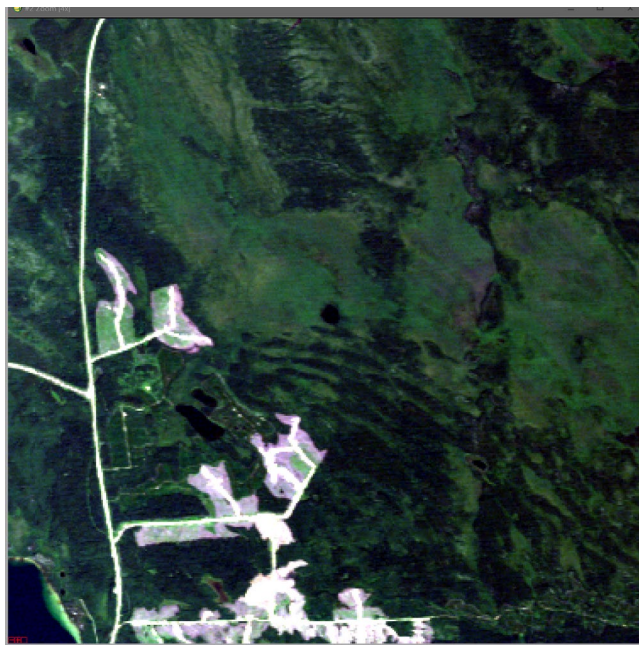


Figure 3. Linear stretched RGB radiance images simulated by MCSScene for a subset of the Boreal scene for solar zenith angles of 45 (top) and 90 (bottom) degrees.

III. TARGET DETECTION RESULTS

The scenes in Figures. 2 and 3 have been atmospherically compensated to scene reflectance using the in-scene code QUAC [10]. The standard Adaptive Coherence Estimator (ACE) [11] detector was then used to evaluate detection performance for the scenes using a pure target reflectance signature. For the scene shown in Figure 2, Figure 4 shows the Receiver-Operator Curves (ROC) for the detection of 400 subpixel targets varying from a fill-factor of 2% to 10%. Targets make up fewer than 0.18% of the pixels in the scene, perhaps most importantly the scene covariance can be calculated without significant impact from the targets that are present. There is decreased target detection performance for scenes with lower illumination primarily due to the increased importance of the scene noise as the illumination decreases. The spectral at sensor radiance at sunset is approximately four orders of magnitude below the signal when the scene is fully sunlit, but 80% of the targets are still detected with a false alarm rate of 10^{-2} [12].

Figure 5 shows the ROC plots for the Boreal scene with the same embedded subpixel target as was used in the Blind-Test scene. In this figure we plot the detection rate for solar zeniths of 0, 45 and 90 degrees for the high visibility simulations. We have also added a curve for the detection results for a 90-degree solar zenith angle case with a visibility of 23 km, labeled hazy in the figure. The detection results improve as the visibility is lowered from 100 km to 23 km. This result may seem counter intuitive, but the additional aerosol leads to more scattering which in this scenario increase the number of photons reaching the ground, thus improving the detection results. Figure 6 shows the linearly stretched RGB image for the 23 km visibility case. Examination of the detailed spectral data across these

two 90-degree solar zenith scenes indicates that the additional scattering tends to increase the radiance in the NIR and SWIR part of the spectrum. The blue target spectrum has a significant SWIR feature which would be more easily detected with the enhanced SWIR radiance. This specific result is very dependent on the target spectral signature and its contrast to the scene elements.

IV. CONCLUSIONS AND FUTURE WORK

In this paper, we report initial results for an ongoing study of rare spectral target detection statistics under low light conditions. To explore this problem a first-principles simulation model for spectral imagery was used. This model is based on a DSMC radiative transport approach. The code, named MCScene, has been successfully validated through comparisons with exact scattering calculations, and its utility has been demonstrated in applications to remote sensing problems. Recent upgrades to MCScene allow simulation of low light and twilight conditions. Subpixel spectral targets were embedded in the scene reflectance maps before simulating the scene radiance under different illumination conditions. The low light simulations indicate that target detection even under twilight conditions is possible given sufficient sensor signal to noise and target to background spectral contrast.

ACKNOWLEDGMENT

The authors wish to acknowledge Spectral Sciences, Inc. for support under an internal research and development grant.

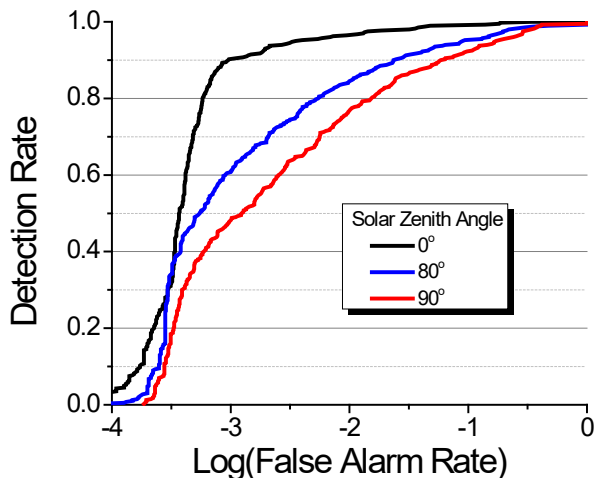


Figure 4. ROC curves for blue roof subpixel targets in the RIT Blind-Test Scene simulated by MCScene using QUAC atmospheric correction followed by the ACE detection algorithm.

REFERENCES

[1] K. Kirschner, <https://payloadspace.com/blacksky-reports-q1-results>, accessed: 2024-03-31
 [2] S. Richtsmeier, A. Berk, S. M. Adler-Golden, and L. S. Bernstein, "A 3D Radiative-Transfer Hyperspectral Image Simulator for Algorithm Validation," Proceedings of ISSSR 2001, Quebec City, Canada (June 2001).

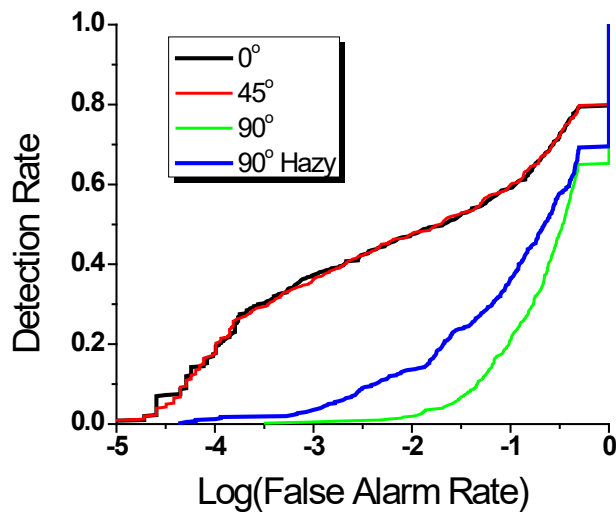


Figure 5. ROC curves for blue roof subpixel targets detected in the Boreal scene simulated by MCScene after QUAC atmospheric correction followed by the ACE detection algorithm.

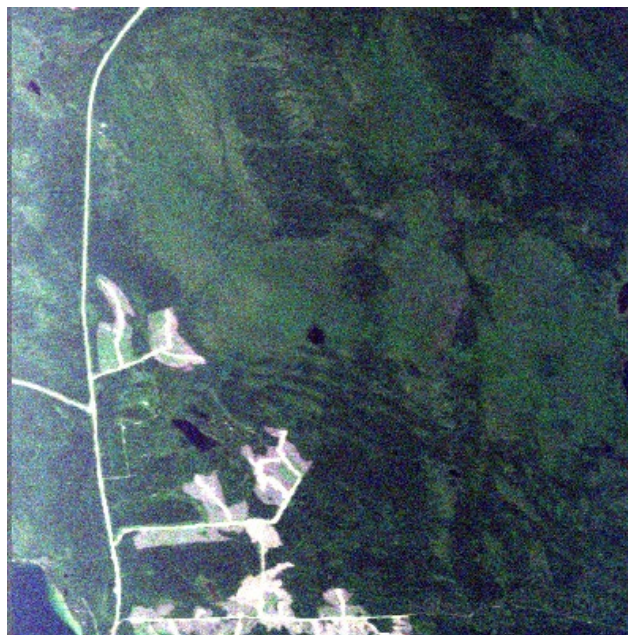


Figure 6. Linear stretched RGB radiance image simulated by MCScene for a subset of the Boreal scene for solar zenith angles of 90 degrees and a visibility of 23 km.

[3] S. Richtsmeier, R. L. Sundberg, R. Haren, and F. O. Clark, "Fast Monte Carlo Full Spectrum Scene Simulation," Proc. SPIE 6233, (2006).
 [4] A. Berk, S. Richtsmeier and R. Sundberg, "Limb-viewing hyperspectral image simulation based on a polygonal earth cross-section (PEX) model," 2017 IEEE International Geoscience and Remote Sensing Symposium (IGARSS), Fort

- Worth, TX, USA, 2017, pp. 1449-1452, doi: 10.1109/IGARSS.2017.8127239.
- [5] USGS, <https://apps.nationalmap.gov/downloader>, accessed: 2024-04-01
- [6] A. Berk, et al., "MODTRAN6: a major upgrade of the MODTRAN radiative transfer code," Proc. SPIE, Algorithms and Technologies for Multispectral, Hyperspectral, and Ultraspectral Imagery XX, 90880H (June 13, 2014); doi:10.1117/12.2050433.
- [7] J. P. Kerekes and D.K. Snyder, "Unresolved target detection blind test project overview," Proc. of SPIE Vol. 7695 769521-1 (2010).
- [8] R. Green, et al., "AVIRIS Land-Surface Mapping in Support of the Boreal Ecosystem-Atmosphere Study," 2000-01-012, <https://ntrs.nasa.gov/citations/20020014837>, accessed: 2024-04-01.
- [9] T. Cocks, R. Janssen, A. Stewart, I. Wilson, and T. Shields, 1998, "The HyMap Airborne Hyperspectral Sensor: The System, Calibration and Performance," Proc. 1st EARSeL Workshop on Imaging Spectroscopy (M. Schaepman, D.Schlöpfer, and K.I. Itten, Eds.), 6-8 October 1998, Zurich, EARSeL, Paris, pp. 37-43.
- [10] L. S. Bernstein, X. Jin, B. Gregor, and S. Adler-Golden, "The Quick Atmospheric Correction (QUAC) code: algorithm description and recent upgrades," Opt. Eng. 51(11), 111719 (2012). doi:10.1117/1.OE.51.11.111719
- [11] S. S. Kraut, L. L. Scharf, and R. W. Butler, "The Adaptive Coherence Estimator: A uniformly most-powerful invariant adaptive detection statistic," IEEE Trans. Signal Processing, Vol. 53, No. 2 (2005).
- [12] R. L. Sundberg "The impact of topographic shadows on subpixel target detection", Proc. SPIE 12688, Imaging Spectrometry XXVI: Applications, Sensors, and Processing, 1268803 (20 October 2023), doi:10.1117/12.2675427

Improved Method for Telemetry Data Processing in LEO Satellite

Dongseok Chae

Satellite Technology Research & Development Division
 Korea Aerospace Research Institute
 Daejeon, Korea
 email: dschae@kari.re.kr

Abstract—Satellite telemetry data is typically gathered using predefined telemetry data tables. Upon selecting data groups for collection, the same data from the chosen packets is repetitively gathered at predetermined intervals, irrespective of the satellite's operational status. However, in the event of specific errors during satellite operations or transitions to particular states, it becomes imperative to include specific data corresponding to the satellite's state or to modify the collection frequency of certain data sets. Given the constrained contact time and communication speed of low-Earth orbit satellites, complete data transmission may not be feasible under adverse communication conditions or when the satellite is in a safe mode. Therefore, a functionality is essential to selectively transmit only the indispensable data contingent upon the prevailing circumstances. This paper provides an overview of the telemetry data processing methodology utilized for low-Earth orbit satellites developed in Korea and outlines mechanisms for automatic adjustment of telemetry data in alignment with the satellite's operational status. Additionally, it presents various strategies for selectively transmitting essential data based on the prevailing conditions.

Keywords—telemetry; downlink; playback.

I. INTRODUCTION

The telemetry data is categorized into specific packet groups based on data type, and the designated items for each packet are collected every second according to a predefined telemetry data table, then stored in mass memory. These stored data are transmitted to the ground in the form of playback data, along with real-time data, during ground communication [1]. Table 1 illustrates the protocols governing the generation and transmission of telemetry data.

TABLE I. THE RULES FOR TELEMETRY DATA PROCESSING

Telemetry Format	Consultative Committee for Space Data Systems (CCSDS) [2][3]
Downlink Rate	4.096 Kbps (Low), 1.5625 Mbps (High)
CADU / VCDU Size	256 / 220 Bytes
Packet Group	State Of Health (SOH1~SOH4), Precise Orbit Determination Data (POD), Precise Attitude Determination Data (PAD) Payload Telemetry (PLD),
Mass Memory Size	4 Gbits
Playback Downlink	756 VCDUs per second
Telemetry Tables	Master Telemetry Table (MTT), Packet Sequence/Contents Table (PST, PCT)

Figure 1 shows telemetry format and Figure 2 shows the table driven telemetry acquisition.

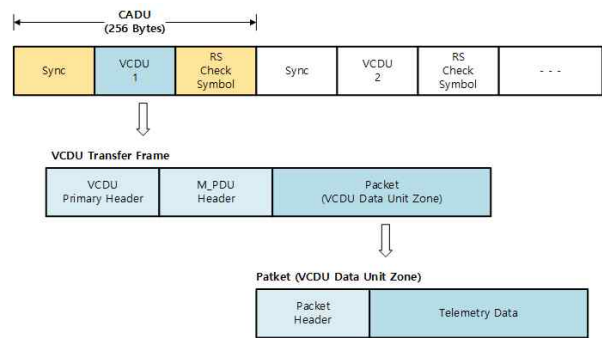


Figure 1. Telemetry Format

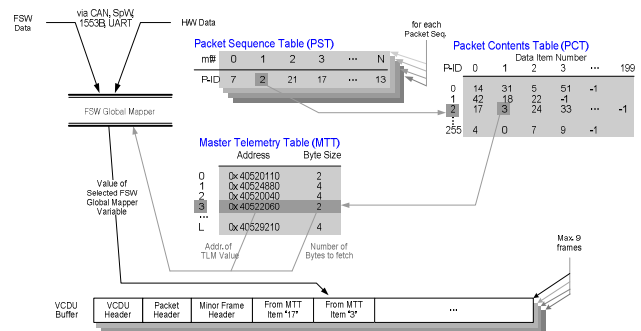


Figure 2. Table Driven Telemetry Acquisition

Given the limited storage capacity of the satellite's mass memory and the constrained transmission speed during communication, the duration of data storage is determined based on the significance of each data item, ensuring it does not surpass the capacity limit. The storage duration ranges from 1 to 32 seconds, varying accordingly. Upon selection of a packet group by the ground, data collection ensues as per a predefined data table. Once the data group is chosen, the selected packet data are repetitively collected at fixed intervals. However, in the event of specific errors or state transitions during satellite operation, certain data may become redundant or require less frequent collection, while others may necessitate inclusion or a shorter collection cycle.

In such scenarios, it is imperative to eliminate redundantly generated data depending on the satellite's status, include essential data, or adjust the cycle of specific data. To address this requirement, a functionality is needed to monitor the satellite's status and automatically modify telemetry data packets to collect the requisite data in accordance with the prevailing state.

Furthermore, low-Earth orbit satellites store all telemetry data generated in a mass memory in the sequential order of generation. Subsequently, the accumulated telemetry data is transmitted collectively to the ground control system during communication with the ground. Figure 3 illustrates the process by which telemetry data is stored and downlinked via the mass memory [1].

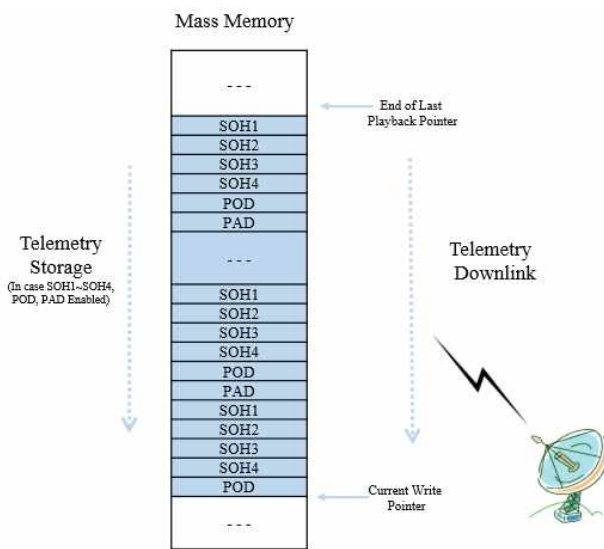


Figure 3. Telemetry Data Storage and Downlink Example

Nevertheless, due to the extremely limited communication time, while all data may be transmitted under normal circumstances, it may not be feasible to transmit all data if the communication environment is compromised or the satellite is in safe mode. In such instances, there is a need for a functionality to selectively transmit only the essential data contingent upon the prevailing circumstances.

In essence, to address challenges stemming from restricted storage capacity, limited contact time, and downlink transmission speed, the storage phase should employ adaptable data formats tailored to the satellite's status. This ensures the storage of as much pertinent data as possible. Similarly, in the transmission phase, the inclusion of a functionality capable of transmitting only essential data becomes imperative.

This paper outlines the pertinent methodologies. Section II delineates the telemetry acquisition approach predicated on the satellite's status. Section III expounds upon the enhanced telemetry storage and downlink methodologies aimed at selectively transmitting solely the indispensable

data. Lastly, Section IV encapsulates the conclusions drawn and outlines avenues for future research.

II. TELEMETRY ACQUISITION BASED ON SATELLITE STATUS

The fundamental processing concept of the telemetry data acquisition method, contingent upon the satellite's status, is illustrated in Figure 4. Under normal circumstances, data predetermined or ordered by the ground are collected. However, if the satellite's state transitions to a specific condition or encounters predefined errors, a procedure is initiated to exclude redundant data packets while automatically incorporating essential ones. This process can be executed through the utilization of the satellite's Relative Time Command Sequence (RTCS) processing function [4].

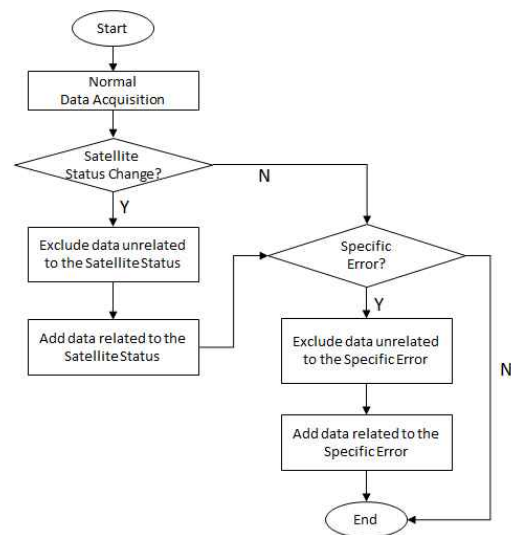


Figure 4. Basic Concept of Telemetry Acquisition

TABLE II. TELEMETRY PACKET SEQUENCE BY SATELLITE STATUS

TM Group	Packet Sequence (by Satellite Status)			
	Normal	State #1	State #2	State #3
SOH1	PKT1, PKT3 PKT3, PKT4	PKT1, PKT2 -	- PKT3, PKT4	PKT1, PKT2
SOH2	PKT5, PKT6 PKT7	PKT5, PKT6 -	- PKT7	PKT5, PKT6 -
SOH3	PKT8 PKT9	- PKT9	- PKT9	- PKT9
SOH4	- -	PKT10, PKT11 -	- PKT12, PKT13	PKT10, PKT11 PKT12, PKT13
POD	POD	POD	-	POD
PAD	PAD	PAD	PAD	-
PLD	PLD	-	-	PLD

Table 2 presents an illustrative example of how telemetry data packets may vary depending on the specific state of the satellite. Under normal operating conditions, the SOH1 group comprises PKT1, PKT2, PKT3, and PKT4 packets, the SOH2 group contains PKT5, PKT6, and PKT7 packets, the SOH3 group consists of PKT8 and PKT9 packets, and packets from the POD, PAD, and PLD groups are collected. However, when the satellite transitions to a particular state (State #1), PKT3, PKT4, PKT7, PKT8, and PLD packets are excluded, while PKT10 and PKT11 packets from the SOH4 group are added. PKT10 and PKT11 packets encompass critical data required for monitoring and assessment during State #1.

Incorporating a functionality that automatically adjusts data collection according to the satellite's operational state can significantly enhance the accuracy of satellite status analysis. By excluding superfluous data and selectively including pertinent data, this approach enables more focused analysis while maintaining consistent data volume. Consequently, it facilitates more precise insights into the satellite's condition without imposing additional strain on data storage and computational resources. Moreover, it enhances the overall reliability and responsiveness of satellite monitoring and control systems.

III. IMPROVED TELEMETRY STORAGE AND DOWNLINK METHOD

To establish a functionality capable of swiftly transmitting solely the requisite data contingent three potential methods can be contemplated. Method 1, as depicted in Figure 5, adheres to the previous storage protocol. During transmission, each data type is discerned, and solely the pertinent data is transmitted. While this approach maintains the existing system to a significant extent, it entails extensive processing time. This is because, during transmission, data must be read and verified in frame units, and only the relevant data must be selected and transmitted.

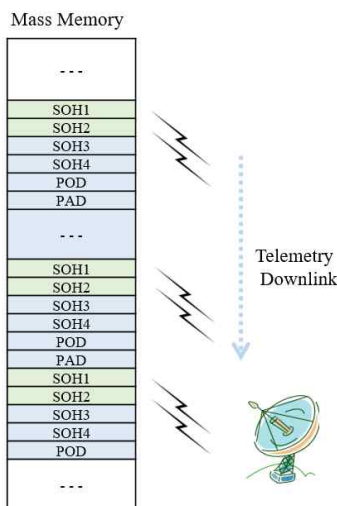


Figure 5. Basic Concept for Telemetry Acquisition (Method 1)

Method 2 involves the utilization of separate memory areas for each data type, as depicted in Figure 6. In this approach, it is presumed that SOH data is stored in Block 1, POD in Block 2, PAD in Block 3, and PLD in Block 4. While this method enables the transmission of only necessary data to the ground in necessary situations, it necessitates the separate management of pointers for each block. Additionally, the size of the memory block must be appropriately allocated in accordance with the data type.

Method 3 involves storing data of the same type on each page, as depicted in Figure 7, and managing it with a data table stored in each page. Data is stored in chronological order, but each page contains the same type of data. For example, SOH data is stored in Pages 1 to 3, POD in Page 4, PAD in Page 5, PLD in Page 6, and SOH data is stored again in Page 7. By maintaining a record of the type of data stored in each page within the page table, it becomes possible to classify and transmit only the necessary data based on the prevailing situation. While Method 3 is somewhat more intricate than Option 2, it eliminates the need to consider memory allocation size for each data type.

Mass Memory

SOH1	SOH2	SOH3	SOH1	SOH2	SOH3	SOH1	SOH2	SOH3	SOH1
SOH2	SOH3	SOH4	SOH1	SOH2	SOH3	SOH4	SOH1	SOH2	SOH3
SOH1	SOH2	SOH3	SOH4	SOH1	SOH2	SOH3	---		
(Block 1)									
POD	POD	POD	POD	POD	POD	POD	POD	POD	POD
POD	POD	POD	POD	POD	POD				
(Block 2)									
PAD	PAD	PAD	PAD	PAD	PAD	PAD	PAD	PAD	PAD
PAD	PAD								
(Block 3)									
PLD	PLD	PLD	PLD	PLD	PLD	PLD	PLD	PLD	PLD
PLD	PLD	PLD	PLD						
(Block 4)									

Figure 6. Basic Concept for Telemetry Acquisition (Method 2)

Mass Memory

(Page #)	1	2	3	4	5	6	7	8	9	10
SOH1	SOH1	SOH1	POD	PAD	PLD	SOH1	POD	SOH1	PAD	
SOH2	SOH2	SOH2	POD	PAD	PLD	SOH2	POD	SOH2	PAD	
SOH3	SOH3	SOH3	POD	PAD	PLD	SOH3	POD	SOH3	PAD	
---	---	---	---	---	---	---	---	---	---	
SOH1	SOH1	SOH1	POD	PAD	PLD	SOH1	POD	SOH1	PAD	
SOH2	SOH2	SOH2	POD	PAD	PLD	SOH2	POD	SOH2	PAD	
SOH3	SOH3	SOH3	POD	PAD	PLD	SOH3	POD	SOH3	PAD	
(Page #)	11	12	13	14	15	16	17	18	19	20
SOH1	PLD	SOH1	POD	SOH1	PAD	SOH1	POD			
SOH2	PLD	SOH2	POD	SOH2	PAD	SOH2				
SOH3		SOH3	POD	SOH3		SOH3				
---		---	---	---		---				
SOH1		SOH1	POD	SOH1		SOH1				
SOH2		SOH2	POD	SOH2						
SOH3		SOH3	POD	SOH3						
(Page Table)	SOH	SOH	SOH	POD	PAD	PAD	SOH	POD	SOH	PAD
SOH	PLD	SOH	POD	SOH	PAD	SOH	POD	-	-	
-	-	-	-	-	-	-	-	-	-	

Figure 7. Basic Concept for Telemetry Acquisition (Method 3)

Each method has its own set of advantages and disadvantages. However, in the current system, Method 1 is considered the simplest and most practical option for implementing the necessary functionality. Nevertheless, to ensure the effectiveness and efficiency of the chosen method, it is essential to conduct an analysis of the software timing that governs its functions.

IV. CONCLUSION AND FUTURE WORK

Given the constraints of limited memory size and communication time inherent to low-orbit satellites, it becomes imperative to generate meaningful data aligned with the satellite's status, rather than redundantly transmitting data. Furthermore, the capability to swiftly transmit only essential data in response to the prevailing situation is indispensable. Several methods to address this challenge have been outlined. To implement this functionality effectively, a comprehensive assessment is required, taking into account the existing flight software's downlink driving method and its integration with hardware functions.

In future efforts, detailed analyses of each method will be conducted to identify the most appropriate approach. Additionally, for transmitting stored data, consideration is being given to designating a memory area and implementing

a method for transmitting data from the satellite corresponding to a specific time designation.

REFERENCES

- [1] D. S. Chae, "Telemetry Storage and Downlink Management for a LEO Satellite", SPACOMM, Feb. 2014, pp. 18-21.
- [2] CCSDS 102.0-B-5 Consultative Committee for Space Data Systems Packet Telemetry, Nov. 2000
- [3] CCSDS 873.0-M-1, Spacecraft onboard interface services—file and packet store services, Sep. 2011.
- [4] Y. S. Youn, "Command Design For Low Earth Orbit Satellite", SASE 2017 Fall Conference, 2017, pp. 450-451.
- [5] J. R. Wertz and W. J. Larson, Space Mission Analysis and Design, Third edition, Microcosm Press, Torrance Ca, USA, 1999.
- [6] G. Casperson, "Software System Development for Spacecraft Data Handling & Control", TERMA Electronics AS, 1999.
- [7] D. S. Chae, "Playback Data Analysis Utility for a LEO Satellite", SPACOMM, Feb. 2016, pp. 23-26.
- [8] Ashley Carlton, Rachel Morgan, Whitney Lohmeyer, and Kerri Cahoy, "Telemetry Fault-Detection Algorithms: Applications for Spacecraft Monitoring and Space Environment Sensing", Journal of Aerospace Information Systems Volume 15, No. 5, May 2018, pp. 239-252.
- [9] L. Yang, Y. Ma, F. Zeng, X. Peng, and D. Liu, "Improved deep learning based telemetry data anomaly detection to enhance spacecraft operation reliability", Microelectronics Reliability volume 126, Nov. 2021